Polymer 328 (2025) 128358

Contents lists available at ScienceDirect

Polymer

journal homepage: www.elsevier.com/locate/polymer

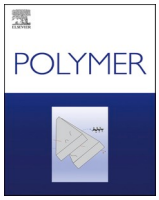

Inelastic and quasielastic neutron scattering on polynorbornenes with bulky carbocyclic side groups

Paulina Szymoniak [a], Mohamed A. Kolmangadi [a,1], Martin Böhning [a], Nicolas R. De Souza [b], Fanni Juranyi [c], Reiner Zorn [d], Andreas Schönhals [a,e,*]

[a] Bundesanstalt für Materialforschung und -prüfung (BAM), Unter Den Eichen 87, 12205, Berlin, Germany
[b] Australian Nuclear Science and Technology Organisation (ANSTO), New Illawarra Road, Lucas Heights, NSW, 2234, Australia
[c] PSI Center for Neutron and Muon Sciences, 5232, Villigen PSI, Switzerland
[d] Forschungszentrum Jülich GmbH, Jülich Centre for Neutron Science (JCNS-1), 52425, Jülich, Germany
[e] Institut für Chemie, Technische Universität Berlin, Straße des 17. Juni 135, 10623, Berlin, Germany

A B S T R A C T

This study investigates the molecular mobility and vibrational properties of polynorbornenes with bulky carbocyclic side groups using inelastic and quasielastic neutron scattering techniques. The polymers, synthesized via metathesis and addition polymerization, exhibit varying degrees of microporosity, which significantly influences their gas separation performance. By inelastic neutron scattering experiments, it could be shown that all considered polymers have excess contributions to the low frequency vibrational density of states known as the Boson peak. The maximum frequency of the Boson peak correlates to the microporosity of the polymers. This correlation supports the sound wave interpretation of the Boson peak, suggesting that the microporous structure enhances the compressibility of the material at a microscopic length scale. The molecular mobility, particularly the methyl group rotation, was characterized using elastic scans and quasielastic neutron scattering. The study revealed a temperature dependent relaxation process, with the onset of molecular fluctuations observed around 200 K for the polymer containing methyl groups. For the polymer having no methyl groups only elastic scattering is observed. The methyl group rotation was analyzed in terms of a jump diffusion in a threefold potential with three equivalent energy minima. This leads to an almost correct description of the q dependence of the elastic incoherent scattering function when the number of hydrogen nuclei undergoing the methyl group rotation is considered. It was further evidenced that the fraction of methyl undergoing the methyl group rotation increases with increasing temperature.

1. Introduction

In chemical and related industries, separation processes are central operations. For the separation of gasses, classical technologies based on adsorption or cryogenic distillation are often employed. However, these approaches are costly, energy consuming, and mechanically demanding. For the future, where more sustainable energy is needed, these conventional technologies must be replaced by energy- and cost-effective processes.

Membrane based separations using polymers for the active separation layer represents a novel and green approach for gas separation. In addition to being cost- and energy-efficient, membrane processes are easily scalable, so, for example, they can be employed for the purification of natural gas on a large scale, as well as for the upgrading of biogas on a much smaller scale. Another application of membrane processes is the separation of hydrogen and methane distributed simultaneously in urban gas grids. For these applications, the polymer used in the separation layer should exhibit high permeability (flux) and good selectivity for the gas pair in question (e.g. hydrogen and methane) [1,2].

Currently, the most promising materials for the separation layer of membranes are glassy polymers. To provide a high permeability the considered polymers should have a high fractional free volume. The requirement of a high fractional free volume is motivated by solution diffusion model which is generally accepted for the transport of gases in dense polymers [3]. In this approach besides the sorption of gas molecules they diffuse through the polymer film controlled by a diffusion coefficient. As molecular transport mechanism for such a diffusion process consecutive jumps of the gas molecules between free volume sites within the polymer bulk are considered. As for these jump events the formation of temporary channels between the free volume sites is required, the diffusion is related to the molecular mobility of the polymer matrix surrounding the gas molecule. Therefore, a need exists to investigate the molecular mobility of polymers in order to understand

* Corresponding author.BAM Bundesanstalt für Materialforschung und -prüfung (Department Materials Chemistry), Unter den Eichen 87, 12205, Berlin, Germany.
E-mail address: Andreas.Schoenhals@bam.de (A. Schönhals).
[1] Physics & Material Science EMEA, Covestro Deutschland AG, 51373 Leverkusen, Germany.

https://doi.org/10.1016/j.polymer.2025.128358
Received 29 January 2025; Received in revised form 27 March 2025; Accepted 3 April 2025
Available online 5 April 2025

the fundamentals of gas separation processes in addition to the thermodynamic quantities influencing the gas transport.

The idea that the gas transport in dense polymers is mainly determined by the fractional free volume on the one hand, as well as to the molecular mobility on the other hand, opens two different strategies to improve polymers for such processes. The first main direction to tune macromolecular systems for gas separation is to optimize the molecular mobility of polymers in the glassy state [4–6]. For instance, Alentiev et al. described homologous series of Janus-poly (tricyclononenes) synthesized by addition polymerization of norbornene-type monomers [7]. These polymers combine a rigid backbone of norbornene repeat units with three flexible alkyl side chains (-Si(OR)$_3$) connected to each repeat unit. Employing a combination methods allows an in-detail characterization of the molecular mobility of that systems [8]. Recently, these Janus-poly (tricyclononenes) were also investigated by inelastic [9] and quasielastic neutron scattering [10]. From the applicational point view these polymers have potential for the separation of longer hydrocarbons [7].

The second way to improve macromolecules for the application in gas separation membranes is the synthesis or development of glassy polymer systems with extraordinary high fractional free volume like poly (trimethylsilylpropyne) (PTMSP) [11] and poly (4-methyl-2--pentyne) (PMP) from the group of polyacetylenes [12,13]. The permeability values of both those polymers are by orders of magnitudes higher than those of conventional glassy polymers like polysulfone or polycarbonate but they have low selectivity values due to the existence of a large, interconnected micropores. However, the search for macromolecules with a high fractional free volume led to new groups of polymers. One of these groups are polymers of intrinsic microporosity also called PIMs [14–17]. PIMs are characterized by large values of Brunauer/-Emmett/Teller (BET) surface areas in the range of several hundred m^2/g due to an interconnected network of micropores with characteristic sizes in the range of 0.5–2 nm [18,19]. The structural features causing the microporosity of PIMs are rigid ladder-type backbones which are contorted, and which includes in cases also spiro-centers. These structures causing an inefficient segment packing when a condensed state is reached from a solution. In addition to PIMs, also addition polymerized polynorbornenes often exhibit significant microporosity with large BET surface areas. Examples for such polymers can be found elsewhere [20–25]. In the case of these materials the microporosity arises from a semi-rigid mainchain in combination with bulky, sterically demanding side groups. PIMs as well as microporous polynorbornenes show high permeability values together with reasonable selectivities. The latter property is currently not well understood as from the microporous structure a more Knudsen-like diffusion is expected which is less selective. However, it was recently shown for a selected PIM that the diffusion of small molecules (H_2, He) obeys a Knudsen-like behavior, whereas the behavior of larger gas penetrants follows the solution diffusion mechanism [26]. This size-dependent transition was discussed in such a way that for larger gas molecules (O_2, N_2, CO_2 or CH_4) there is a need that bottlenecks between adjacent free volume sites have to be opened and/or closed to allow for a selective transport. Such a process can be also explained in the context of the random gate model by Kanaya et al. [27]. Nevertheless, this establishes a further reason why the molecular mobility in polymers is relevant for separation membranes and should be investigated.

It is well known that the glass transition of polymers is related to the molecular mobility. However, for PIMs and microporous polynorbornenes no glass transition could be detected before the degradation of the polymer by conventional calorimetric methods. To circumvent this problem fast scanning calorimetry (FSC) with heating rates up 10^5 K/s can be employed [28–30] decoupling the time scales responsible for glass transition and degradation. For instance the archetypal PIM-1 shows a glass transition at 644 K at a heating rate of 10^4 K/s [28,29]. Moreover, broadband dielectric spectroscopy can be utilized to investigate the molecular mobility in the considered polymers. In contrast to calorimetric experiments, with this method also more localized fluctuations can be investigated, and it also allows to characterize physical aging in these systems[31–34]. For these high-performance polymers a variety of dielectric active processes have been observed. Furthermore, one of these processes has been assigned to a Maxwell/Wagner/Sillars polarization due to the blocking of charge carriers at the pore walls.

Also, quasielastic neutron scattering (QENS) was employed to investigate the molecular mobility on microscopic time and length scales in such systems relevant for gas transport and separation. Early studies of Kanaya et al. examined polyacetylenes as sample systems [27,35,36]. By these investigations, evidence was provided that the permeabilities of CO_2 or CH_4 can be correlated to microscopic motions of the polymeric matrix at room temperature in the time range of picoseconds. Further QENS investigations have been carried out on PIM-1 [37] and microporous polynorbornenes [38]. These investigations focused on localized relaxation processes, for instance the methyl group rotation. For instance, localized relaxation processes like the methyl group rotation can open or close bottlenecks between the interconnected pores and so control the occurrence of diffusional jumps, especially for gases with larger kinetic diameters, as discussed in the random gate model and therefore giving rise to a favorable size selectivity of the gas transport. Besides the molecular mobility also the low frequency vibrational density of states was investigated for several PIMs [39,40] and a variety of microporous polynorbornenes where its BET surface area values were varied [41]. The vibrational density of states shows characteristic excess contribution, known as Boson peak. As a result, a correlation between the maximum frequency of the Boson peak and the microporosity characterized by the BET surface area was found. This correlation provides a direct link between microscopic properties and applications.

Here, to extent on the previous research, polynorbornenes with different bulky carbocyclic sides groups are investigated by neutron scattering on microscopic length and time scales. The polymers were obtained by different polymerization techniques which results in a variation of the values of the BET surface area. The investigation considers both vibrations as well as the molecular mobility.

2. Materials and methods

2.1. Materials

The structures of the repeat units of the considered polynorbornenes are given in Fig. 1.

The synthesis of the ZMA materials is given in Refs. [42,43] The polymers ZMA64 and ZMA66 were prepared by metathesis polymerization. ZMA67 was synthesized by addition polymerization. The metathesis polymerization leads to a relatively flexible backbone while the main chain of polymers obtained by addition polymerization is more stiff and rigid. Table 1 gives some molecular details of the synthesized polymers like molecular weights and BET surface area values.

The ZMA materials exhibit distinct gas permeation behaviors driven by their structural and porosity characteristics. ZMA64, characterized by its low BET surface area, results in low diffusion coefficients, as expected, limiting gas transport. In contrast, ZMA66 features a significantly higher BET surface area than ZMA64 and slightly higher for ZMA67, which increases gas diffusion coefficients for most gases, including hydrocarbons, making it suitable for applications demanding a high permeability. While ZMA66 shows higher diffusion coefficients across most gases compared to ZMA67, ZMA67 displays slightly better selectivity for CO_2, attributed to its denser and more rigid structure. Both ZMA66 and ZMA67 demonstrate low solubility for small gases. ZMA66 is therefore better suited for applications requiring high gas permeability values, such as hydrocarbon separation, gas sensing, or storage, where throughput is critical. On the other hand, ZMA67, with its denser and more rigid structure, offers greater selectivity,

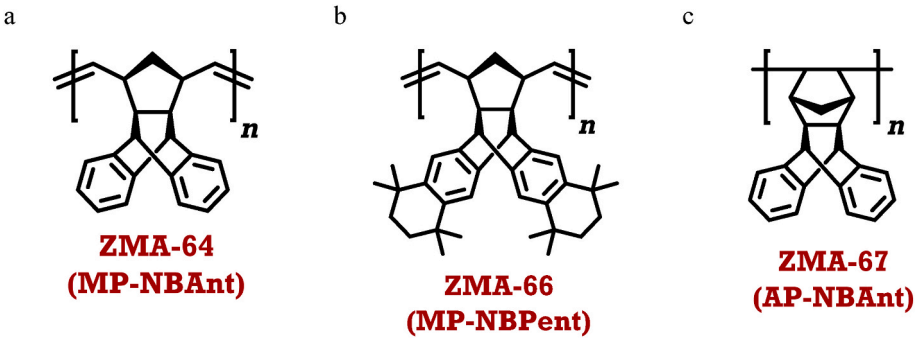

Fig. 1. Chemical structure of the repeating unit of the considered polymer: a – ZMA64, b – ZMA66 and c - ZMA67. The names given in brackets corresponds to the sample given in Refs. [42,43].

Table 1
Molecular weight M_w, Polydispersity and BET surface area values. The data were taken from refs. 44,45.

Code	M_w 10^5 [g/mol]	PDI	BET surface area [m^2/g]
ZMA64	22	3.0	1.3
ZMA66	13	3.2	740
ZMA67	3	2.5	640

particularly for CO_2, making it more suitable for applications where CO_2 capture or controlled storage with limited permeability is required [42,43].

For the film preparation the samples are dissolved in toluene. To reduce the influence of multiple scattering events, the thickness of the final prepared film sample should allow for approximately 10 % of neutron scattering. For this purpose, the concentration of the solution was adjusted. The solution was shaken for 5 h. Then it was cast in a PTFE mold after filtering with a PTFE filter with pores of 0.2 μm. A closed chamber saturated with the vapor of the solvent was employed to control the evaporation of the solvent in the initial stages. The sample was placed in that chamber at room temperature for 3 days to form a film. After this initial process the formed film was moved into a vacuum oven with an oil-free vacuum and annealed at 393 K for three days. By this procedure a complete solvent removal was achieved. The final thicknesses of the samples were: ZMA64 – 0.156 mm (6.8 % expected scattering); ZMA66 – 0.141 mm (9.3 % expected scattering) and ZMA67 – 0.132 mm (9.1 % expected). scattering.

For the neutron scattering experiments the samples were sealed by electro-welding in flat aluminum containers, as Al is nearly transparent for neutrons.

2.2. Neutron scattering

In the neutron scattering experiments carried out here, the momentum and energy exchange between the neutrons and the nuclei of the material under investigation is considered. Therefore, from the experiments information in space and time is obtained for the process of interest [44]. The spatial and temporal content of the experiment is expressed as the double differential cross section defined by

$$\frac{d^2\sigma}{d\Omega d\omega} = \frac{1}{4\pi}\frac{\boldsymbol{k_f}}{\boldsymbol{k_i}}\left(\sigma_{coh}S_{coh}(\boldsymbol{q},\omega) + \sigma_{inc}S_{inc}(\boldsymbol{q},\omega)\right) \quad (1)$$

Equ. 1 is given in the frequency representation where the angular frequency ω is related to the measured energy transfer ΔE by $\omega = \Delta E/\hbar$ (ħ is the Planck constant divided by 2π). The neutron beam is characterized by its incident and final wave vectors $\mathbf{k_i}$ and $\mathbf{k_f}$. The difference of both wave vectors gives the scattering vector $\mathbf{q} = \mathbf{k_f} - \mathbf{k_i}$. Because of isotropy, only the modulus of the scattering vector, q, is considered in the following. The coherent and incoherent dynamic structure factors are denoted by S_{coh} (q,ω) and S_{inc} (q,ω). Ω describes the solid angle of detection. σ_{coh} and σ_{inc} are the scattering cross-sections for coherent and incoherent scattering. All ZMA materials contain only carbon (C) and hydrogen (H) (see Fig. 1). The calculation and the values of σ_{coh} and σ_{inc} are given in the Supporting Information. From the comparison of σ_{coh} and σ_{inc} it is concluded that the scattering is predominantly incoherent.

For the neutron scattering experiments, different techniques have been used. These techniques include inelastic neutron scattering to measure the low frequency vibrational density of states (VDOS). To access the molecular dynamics, quasielastic neutron scattering has been carried out. The experiments include elastic fixed windows scans (elastic scans).

2.2.1. Inelastic neutron scattering

The cold neutron time-of-flight spectrometer FOCUS, operated at the Paul Scherrer Institut in Villigen, Switzerland, was used for the inelastic neutron scattering experiment. The incident wavelength of the neutron beam was 5 Å. For the measurement of the VDOS the full width of the 37 mm wide sample (45° angle with respect to the beam) was used. This resulted in an energy resolution (full width at half maximum, FWHM) of 80 … 121 μeV depending on the scattering angle. The energy resolution was estimated by measuring the sample at T = 2 K by assuming that all molecular fluctuations and vibrations are frozen. The VDOS was measured at 50 K to reduce the influence of quasielastic scattering on the measured signal. For these measurements the temperature of the sample was controlled by a helium cryostat.

The data reduction was done using DAVE [45]. For the calculation of the vibrational density of states, detectors were grouped by angle into 20 groups in the range of 16° … 124°, corresponding to elastic scattering vectors of 0.33 … 2.20 $Å^{-1}$. A self-written Python script was used to correct the data for self-shielding effects in a plate. Fig. 2a gives an example for the raw spectra measured at FOCUS for the low frequency vibrational density of states.

2.2.2. Elastic scans and quasielastic neutron scattering

2.2.2.1. Elastic scans. Elastic fixed window scans, or in short elastic scans, on a neutron backscattering instrument with an energy transfer of ΔE≈0 can be used to obtain an overview about the molecular dynamics. The underlying time scale corresponds to the resolution of the spectrometer. The cold neutron backscattering spectrometer Emu operated at the Australian Nuclear and Technology Organization (ANSTO, Lucas Heights, Australia) was used for these experiments. Emu is a backscattering device of the second generation. It was used with Si-111 monochromators/analyzers and a wavelength of λ_0 = 6.271 Å. This configuration results in a q vector range of 0.69 … 1.77 $Å^{-1}$ The energy resolution was about 0.98 … 1.02 μeV (FWHM). The Doppler drive is set at rest for the elastic scans. The scattering at the lowest temperature is used as reference for the analysis of the measurements. Therefore, it was measured with a higher statistic with a counting time of 10 min. The

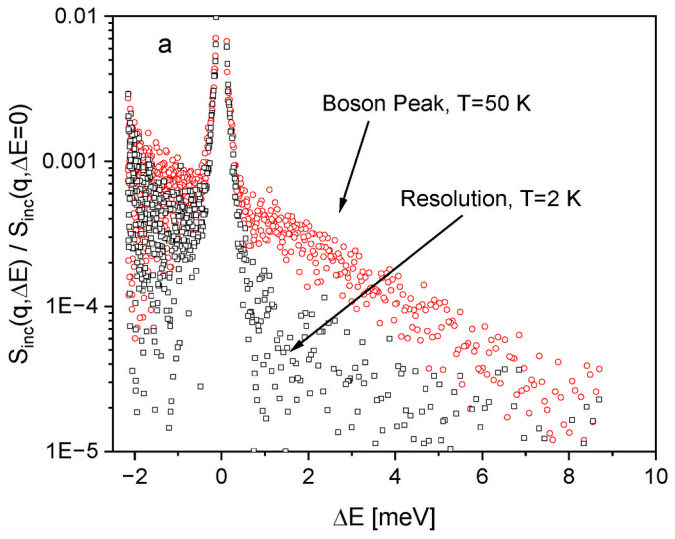

Fig. 2a. FOCUS spectra for ZMA64 at a vector of 1.41 Å^{-1} normalized to the height of the elastic line: Black squares – resolution of FOCUS measured at 2 K. Red circles – Inelastic scattering measured at 50 K. (For interpretation of the references to colour in this figure legend, the reader is referred to the Web version of this article.)

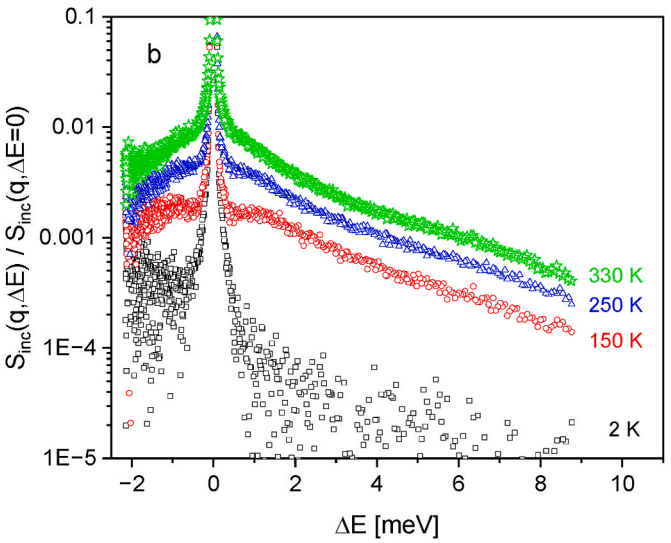

Fig. 2b. FOCUS spectra for ZMA66 at a vector of 1.41 Å^{-1} normalized to the height of the elastic line at the indicated temperatures. The measurement at 2 K serves as resolution for 150 K and 250 K (see text).

temperature scanning rate was 0.94 K/min.

The data reduction was done by a Mathematica script available at ANSTO. From the scattered intensities an effective mean squared displacement is calculated by

$$I_{el}(q,T) / I_{el}(q,2\,K) = \exp\left(-\langle u^2\rangle_{eff} q^2 / 3\right) \quad (2)$$

assuming a Gaussian distribution of displacements. During the analysis multiple scattering is considered as described in Ref. [46]. The amount of multiple scattering is given in the Supporting Information.

2.2.2.2. Quasielastic neutron scattering (QENS). To cover a reasonable time range in the QENS experiments, neutron time-off-flight experiments were combined with neutron backscattering. As the resolutions of the time-of-flight and the backscattering spectrometers are different by ca. two orders of magnitude, S_{inc} (q,ω) obtained from both spectrometers were Fourier transformed and divided by the Fourier transform of the corresponding resolution. The spectra were corrected for multiple scattering. The procedure for the multiple scattering corrections is given in detail elsewhere [47]. The relative contribution of the multiple scattering is given in the Supporting Information. By that way absolute values of the intermediate scattering function S_{inc} (q,t) were obtained, and the data from both spectrometers can be directly analyzed in time domain.

For the shortertime part of the dynamics of the ZMA polymers the time-of-flight spectrometer FOCUS was employed. It was used mainly in the same configuration as described above. To improve the resolution at high angles, the beam size at the samples was reduced by a slit in the front of the sample. A resolution with a maximum FWHM of 91 μeV could be achieved. An example for the measured S_{inc} (q,ΔE) is depicted in Fig. 2b.

To cover a larger temperature range up to 390 K, the sample environment had to be changed on FOCUS. For the low temperature range (2 K, 50 K … 250 K) the helium cryostat discussed for the inelastic measurements had been employed. For the higher temperatures (50 K, 300 K … 390 K) a closed cycle refrigerator was used. The closed cycle refrigerator allows only measurements down to 50 K. This means that the resolution of FOCUS for the measurements in the temperature range from 300 K to 390 K could not be estimated correctly as not all dynamical processes might be frozen as for an estimation at 2 K. To circumvent that problem all the samples were measured at T = 50 K using both cryostats. For the measurements carried out using the closed cycle cryostat alone, only $iFT[S_{inc,T=300\ldots390\,K}(q,\omega)]/iFT[S_{inc,50\,K}(q,\omega)]$ can be calculated where iFT symbolizes the inverse Fourier transformation. But it is desired to calculate S_{inc} (q,t) as $iFT[S_{inc}(q,\omega)]/iFT[S_{inc,2\,K}(q,\omega)]$. This was done by also using the data from the low temperature measurements and calculating as $S_{inc}(q,t) = (iFT[S_{inc,T=100\ldots390\,K}(q,\omega))] / iFT[S_{inc,50\,K}(q,\omega)]) / (iFT[S'_{inc,50\,K}(q,\omega)] / iFT[S'_{inc,2\,K}(q,\omega)])$ where the primes indicate the data from the helium cryostat measurements. The broadening of the spectra in comparison to the resolution indicate the onset of the molecular fluctuations.

For the slower part of the dynamics the neutron backscattering spectrometer Emu was employed. It was used in the same configuration as described above. The doppler drive was set to a maximum speed yielding an energy range of −31 μeV … +31 μeV. Data reduction was carried out by Mantid [48] to obtain four q values in the range 0.69 … 1.77 Å^{-1}. Fig. 2c gives an example for the neutron backscattering measured at Emu. Like for the time-of-flight data the broadening of

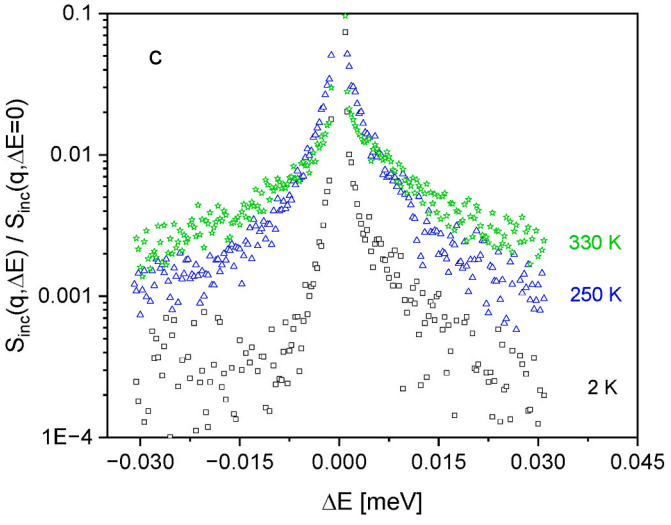

Fig. 2c. Emu spectra for ZMA66 at an angle of 89.4° normalized to the height of the elastic line at the indicated temperatures. The measurement at 2 K serves as resolution.

spectra compared to the resolution indicates the molecular fluctuations.

For ZMA-64, between the low temperature spectrum used as resolution and the higher temperatures a sample change took place. For that reason, the absolute intensities differed by q-dependent factor. The presumed reason is that upon re-insertion in the cryostat the original position could not be exactly reproduced the original position. This was solved by matching the S_{inc} (q,t) from Emu to an extrapolation of the values from FOCUS at the shortest time available from Emu (67 ps).

3. Results and discussions

3.1. Boson peak

For crystalline materials, the Debye model of sound waves predicts for the low frequency vibrational density of states $g(\omega)\sim\omega^2$. In difference to that behavior for amorphous materials like molecular glasses or even polymers characteristic excess contributions to the VDOS are found in the energy range of 1–5 meV. This corresponds to a frequency range of $\omega = 1.5–7.5\ ps^{-1}$. Reducing $g(\omega)$ by ω^2 visualize these excess contributions as a peak, the so-called Boson peak (BP) [49]. There is a general agreement that the Boson peak is a feature of amorphous glasses. Nevertheless, it was also observed for materials with a partial order like plastic crystals (see for examples refs. [50–55]).

The theoretical understanding of the Boson peak is still under a debate. However, there are several groups of theoretical approaches. One of these approaches is the soft potential model. Here, quasi-localized vibrations which only exist for glasses due to their amorphous nature are discussed as the origin of the BP [54–56]. It is worth noting that the quasi-localized modes assumed in the soft potential model are different from sound waves. A further theory to understand the Boson peak starts from the classical sound wave pictures developed for crystals. In that model the Boson peak is considered as a broadened and frequency-shifted version of the Van Hove-singularity of a hypothetical crystalline system due to the amorphous disorder [57]. This can be also discussed as a pseudo Van Hove singularity due to an interaction between the branches of the optical and acoustical dispersion [51]. It is worth noting that in the sound wave approach the Boson peak is related to a transverse sound velocity and a characteristic length scale considering an elastic continuum characterized by a local modulus. (see for example [58–62]). Schirmacher et al. developed a third approach that connects the two aforementioned categories. In this model, the BP is attributed to harmonic vibrations occurring in a disordered environment. These vibrations still exhibit properties of sound waves. Nevertheless, this approach does not consider the BP to be a modification of the Van Hove singularity. Additionally, it aligns with the soft potential model in its conceptualization of "soft spots" [63,64]. Further models of the Boson peak are discussed elsewhere [65–67].

There is some experimental evidence that the BP is related to sound waves[68–72]. Recently the sound wave interpretation was also employed to understand the Boson peak in PIMs [39,40] and microporous polynorbornenes [41] as well as for the Janus-polynorbornenes [71].

The standard expression of one phonon scattering is used in the incoherent approximation to estimate the vibrational density of states from the measured scattering. For one type of nucleus, one obtains [72].

$$S_{inc}(q,\omega) = e^{-2W(q)}\left(\delta(\omega) + \frac{\hbar q^2}{2\overline{m}}\frac{g(\omega)}{-\omega} \times \left(1 - exp\left(\frac{\hbar\omega}{k_B T}\right)\right)^{-1}\right) \quad (3)$$

where $e^{-2w(q)}$ symbolize the Debye/Waller factor. $\overline{m}$ denotes the average mass of an atom. As hydrogen has the highest scattering cross-section but the lowest mass its dynamics is overemphasized in the result. If it is assumed that all hydrogens contribute proportionally to the measured vibration spectra, the estimated g(ω) represents a VDOS in a thermodynamic sense. Generally, the observed scattering Sobs (q,ω) is a convolution of the resolution of the spectrometer R (q,ω) with the scattering from the sample. However, as the BP is a broad feature in the spectra the convolution can be approximated by a sum [73]

$$\begin{aligned} S_{obs}(q,\omega) &= S(q,\omega) \otimes R(q,\omega) \\ &\approx e^{-2W(q)}\left(R(q,\omega) + \frac{\hbar q^2}{2m}\frac{g(\omega)}{-\omega} \times \left(1 - exp\left(\frac{\hbar\omega}{k_B T}\right)\right)^{-1}\right) \end{aligned} \quad (4)$$

When two temperatures are considered (here 2 K and 50 K) equ. 4 defines a linear system of two equations from which g(ω) and R (q,ω) can be calculated. The finally obtained vibrational density of states is obtained as an average of the detectors with elastic q values ranging from 1.2 to 2.2 $Å^{-1}$.

Fig. 3 gives the vibrational low frequency density of states versus in the reduced representation $g(\omega)/\omega^2$. Firstly, for all polymers investigated here, a Boson peak is observed. Secondly, the frequency position of the BP depends on the structure of the material under study.

In refs. 40 and 41 a correlation between the maximum frequency of the Boson peak ω_{BP} and the microporosity characterized by the BET surface area values was discussed in the frame of the sound wave approach to the Boson peak. The sponge-like structure of microporous polymers results in a higher compressibility at a length scale defined by the lowest q value of the neutron scattering experiment. Furthermore, it was shown that the frequency position of the Boson peak depends on the structure of the backbone of the microporous polymers [40].

Fig. 4 depicts the maximum frequency of the Boson peak versus the BET surface area value for the polymers investigated here, but also including literature results for other addition polymerized microporous polynorbornenes [41] and PIMs [40].

Of the polymers investigated here, ZMA64, a metathesis polynorbornene showing no significant microporosity (see Table 1) is located on the left, i.e. at a frequency observed also for other non-porous polymers like Matrimid. Interestingly, the maximum frequency of the Boson peak of the structurally related addition polymer ZMA67 lies on the same continuous curve established by the addition-type polynorbornenes investigated earlier, but due to its higher BET surface area on the right end of this curve.

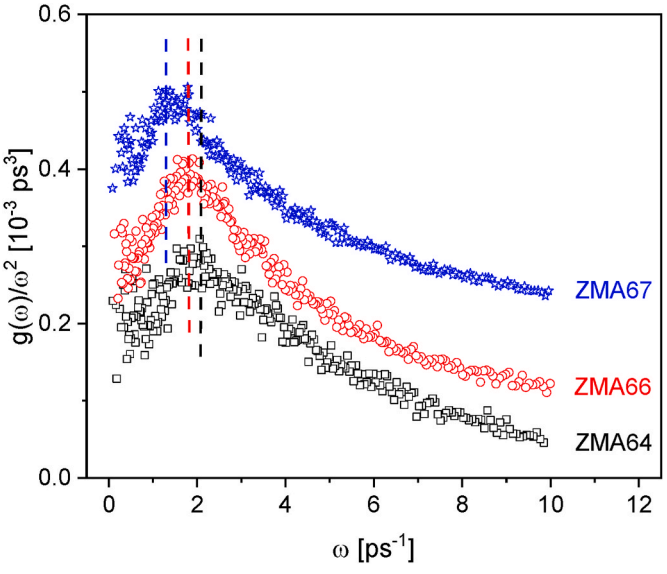

Fig. 3. Vibrational low frequency density of states in the representation g (ω)/ω² versus angular frequency. Black squares – ZMA64; red triangles – ZMA66 and blue asterisks – ZMA67. The dashed lines mark the maximum positions of the Boson peak. The curves are shifted along the y-scale for sake of clearness (ZMA66 + 0.05; ZMA67 + 0.2). (For interpretation of the references to colour in this figure legend, the reader is referred to the Web version of this article.)

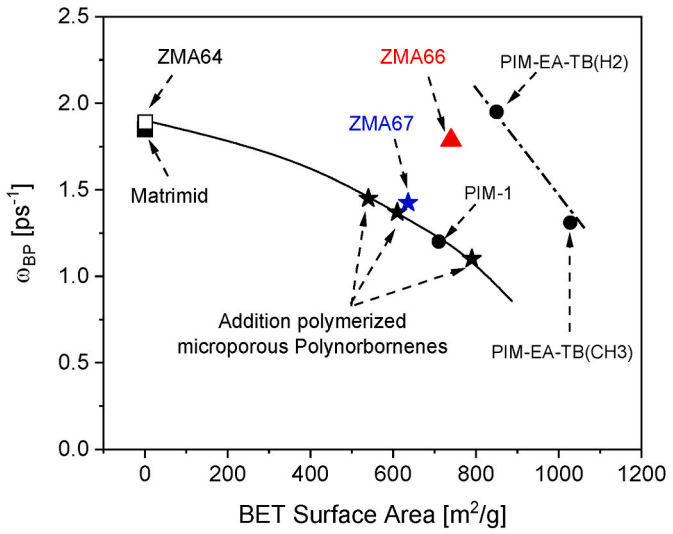

Fig. 4. Maximum frequency of the Boson peak versus the BET surface area. Open square – ZMA64; red triangle – ZMA66; blue asterisk – ZMA67. The back asterisks are addition polymerized microporous polynorbornenes. The data are taken from ref. 41. The solid data are data for Matrimid [39]. Circles are data for different PIMs where the data for PIM-1 are taken form ref. 39 and data for PIM-EA-TB are taken from ref. 40. The different lines are guides for the eyes. (For interpretation of the references to colour in this figure legend, the reader is referred to the Web version of this article.)

This means the result found here is consistent with the previous data and provides some further evidence for the sound wave interpretation of the Boson peak [41].

The polymer ZMA66 was synthesized by metathesis polymerization. Compared to ZMA67 it has a completely different backbone with a higher flexibility. Therefore, it is not expected that ω_{BP} obeys the correlation line of the addition polymerized microporous polynorbornenes as besides the microporosity of the stiffness of the backbone plays a role for the low frequency vibrational density of states. A similar result was observed for PIMs (see Fig. 4).

3.2. Molecular mobility

The molecular mobility was investigated by elastic scans as well as by QENS for the metathesis-type polynorbornenes ZMA64 and ZMA66, bearing different side groups, only.

3.2.1. Elastic scans

Fig. 5 depicts the temperature dependence of the effective mean squared displacement $<u^2>_{eff}$ for the two metathesis polynorbornenes ZMA64 and ZMA66. For the lowest temperature the linear increase of $<u^2>_{eff}$ with temperature is due to vibrations. In that temperature range there is no remarkable difference in the change of the effective mean squared displacements for both polymeric materials.

With increasing temperature, a step-like change in the temperature dependence of $<u^2>_{eff}$ around 200 K is observed for ZMA66. This step indicates the onset of molecular motions in ZMA66. Besides two additional cyclo-carbon rings in ZMA66, the presence of four methyl groups is the main structural difference compared to ZMA64. It is unlikely that the molecular mobility observed for ZMA66 at around 200 K is due to fluctuations of the cyclo-carbon rings or the segmental fluctuations as the glass transition could not be detected. Therefore, the underlying molecular fluctuations of the step-like change of $<u^2>_{eff}(T)$ are assigned to methyl group rotations. This assignment is supported by ZMA64 having a comparable backbone structure but no methyl groups.

At higher temperature there is a further kink-like change in the temperature dependence of the effective mean squared displacement for both materials. This kink-like change in $<u^2>_{eff}(T)$ corresponds to the onset of further molecular motions besides the methyl group rotation.

The dense structure of ZMA64 and lack of methyl group rotation limit molecular mobility and gas transport, leading to low diffusion coefficients. In contrast, ZMA66 exhibits active methyl group rotation at elevated temperatures, enhancing localized mobility and facilitating efficient gas diffusion by opening bottlenecks between interconnected micropores. The interplay between methyl group dynamics, microporosity, and molecular flexibility plays a crucial role in determining the gas transport properties, with ZMA66 showing a balance between permeability and flexibility [42,43].

3.2.2. Quasielastic neutron scattering

Fig. 6 compares the intermediate time dependent scattering function S_{inc} (q,t) for ZMA64 and ZMA66 at a scattering vector of q = 1.77 $Å^{-1}$ at T = 300 K. For both materials the data measured by neutron time-of-flight scattering and neutron backscattering agree nicely. For the ZMA64 only an elastic scattering independent of time is observed

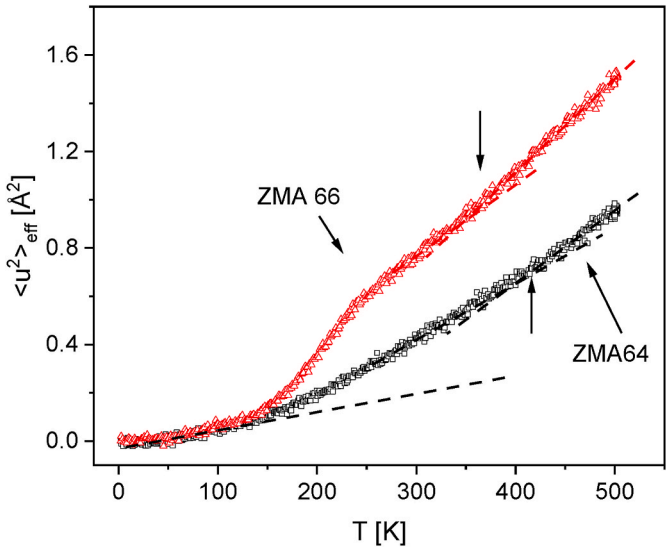

Fig. 5. Temperature dependence of the effective mean squared displacement as indicated. Lines are guides for the eyes.

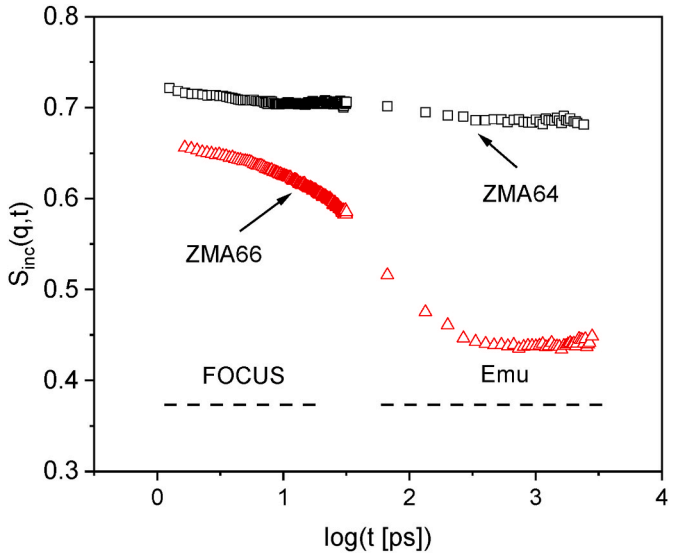

Fig. 6. Incoherent intermediate scattering function S_{inc} (q,t) versus time at T = 300 K for q = 1.77 Å as indicated: The data at short time are measured at FOCUS where that at longer times are obtained from Emu.

indicating the absence of any molecular fluctuations in the considered temperature range. In difference to that behavior the time dependence of S_{inc} (q,t) for ZMA66 reveals a step-like decay evidencing a relaxation process. According to the discussion above, this relaxation process is assigned to the methyl group rotation.

The generally accepted model for the methyl group rotation is the Rotation Rate Distribution Model (RRDM) [74]. In order to ease the analysis here, a simple stretched exponential function is utilized. The employed fit function reads

$$S_{inc}(q,t) = DWF^{*}\left((1 - EISF_M(q))\exp\left(-\left(\frac{t}{\tau_M}\right)^{\beta_M}\right) + EISF_M(q)\right). \quad (5)$$

In equ. 5 DWF denotes the Debye/Waller factor $DWF = \exp(-q^2 < u^2_{fast} > /3)$. The mean squared displacement $\langle u^2_{fast}\rangle$ takes account for fast processes like vibrations. τ_M is the relaxation time for the methyl group rotation, whereas β_M is the corresponding stretching parameter. $EISF_M$ symbolizes the elastic incoherent structure factor for the methyl group rotation. Fig. 7 depicts S_{inc} (q,t) for ZMA66 at T = 300 K for all available q vectors including the fitting function. The figure shows that equ. 5 describes the data well.

The dependence of the $EISF_M$ on the q vector can be calculated straightforwardly by a jump-diffusion assuming a three-fold potential $V(\phi) \sim (1 - \cos(3\phi))/2$ with three equivalent energy minima with respect to the rotation angle ϕ [74,75]. This calculation yields

$$EISF_M(q) = \frac{1}{3}\left(1 + 2\frac{\sin(\sqrt{3}\ qr)}{\sqrt{3}\ qr}\right). \quad (6)$$

r denotes the radius of the circle defined by the positions of the hydrogens in the methyl group. Its value is 1.027 Å.

The estimated values of the $EISF_M$ are plotted versus q in Fig. 8a and compared to the prediction of equ. 6. This comparison reveals that the experimental data do not follow the theoretical expectation. To discuss the discrepancy between the experimental data and the theoretical approach one has to consider the number of hydrogens in the methyl group in comparison to all hydrogens in the repeating unit. ZMA66 has 46 hydrogen nuclei in the repeat unit but only 24 hydrogens in the eight methyl groups. This means 24 hydrogens are visible during the QENS experiment where the rest scatters elastically. Therefore, equ. 6 must be modified considering the theoretical fraction of hydrogens C_{fix} which scatters elastically. C_{fix} is defined by $C_{fix}=(H_{repeating\ unit} - H_{methyl\ groups})/H_{repeating\ unit}$. With this definition equ. 6 is corrected for the number of hydrogens which scatters elastically by [37,38,47,66].

$$EISF_{M,corr}(q) = (1 - C_{fix})EISF_M(q) + C_{fix}. \quad (7)$$

The value of C_{fix} calculated from the chemical structure of the repeating unit is (46-12)/46 = 0.478. Fig. 8a shows that $EISF_{M,\ corr}(q)$ with the theoretical value of C_{fix} is closer to the experimental but still does not describe it correctly. Finally, equ. 7 is fitted to the data yielding to a value of C_{fix} of 0.574. This larger value of C_{fix} compared to the theoretical one indicate that not all methyl groups present in the chemical structure take part in the methyl group rotation.

Fig. 8b compares the q dependence of the EISF of the methyl group rotation for all measured temperatures. This figure reveals that besides the q dependence of the EISF it is also temperature dependent which can be described by a temperature dependent $C_{fix}(T)$. For all temperatures C_{fix} is estimated by fitting equ. 7 to the corresponding data and plotted versus temperature in Fig. 9. Generally, C_{fix} decreases with increasing temperatures. This means that methyl groups that are immobilized at lower temperatures become mobile at higher temperatures. A similar behavior was observed previously for PIM-1 [37]. A closer inspection of the data reveals that the temperature dependence of the relaxation time of the methyl group rotation undergoes a change at ca. 330 K. For higher temperatures, C_{fix} becomes lower than the theoretical value. That behavior cannot be explained only by the methyl group rotation. There must be some additional contributions due to some mobility of the polymer matrix. A similar behavior was also observed for poly (methyl phenyl siloxane) and explained by localized islands of mobility [76]. It is worth mentioning that the data points of C_{fix} which are below the theoretical one are at temperatures above the second kink in the temperature dependence of the effective mean squared displacement. Therefore, the molecular mobility of the ZMA materials should be further investigated for instance by broadband dielectric spectroscopy or dynamical calorimetry.

Finaly from the fit of equ. 5 to the data, a relaxation time for the methyl group rotation can be extracted. As the methyl group relaxation is a localized relaxation process, the relaxation time are independent of the q vector (see SI, Fig. S1). A mean value of the relaxation time is estimated by averaging over the available q vectors. The relaxation time is plotted versus inverse temperature in the activation plot (see Fig. 10). At first glance the temperature dependence of τ seems to roughly follow the Arrhenius equation which reads

$$\tau(T) = \tau_\infty \exp\left(\frac{E_A}{R\,T}\right). \quad (8)$$

Here E_A is the activation energy and R is the general gas constant. From such a fit 17.4 kJ/mol is estimated for the activation energy. The estimated energy corresponds to that estimated earlier for PIM-1 [37,40]. It is worth mentioning that the values of the activation energy obtained for the microporous polymers is higher than those found for polymers with a flexible backbone. This points to some influence of the stiff backbone of the microporous macromolecules on the methyl group rotation.

A closer inspection of the temperature dependence of the relaxation time of the methyl group rotation reveals that there is a subtle change of the slope at ca. 330 K. The temperature range of this change of τ corresponds to that were also a change in the temperature dependence of C_{fix} is observed. From that coincidence one can conclude that both effects are related. As the regression coefficient of the linear regression including all data points is already $R^2 = 1$ no conclusion can be drawn by comparing the regression coefficients of one or two linear fits.

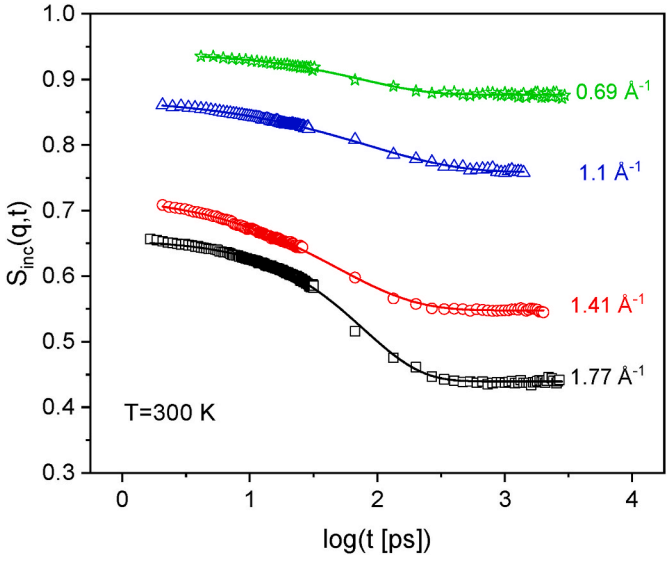

Fig. 7. Incoherent intermediate scattering function S_{inc} (q,t) for ZMA66 versus time at T = 300 K for the indicated q vectors. The lines are fits of equ. 5 to the data.

4. Conclusion

This study successfully demonstrates the critical role of vibrations as well as the molecular mobility and microporosity in the performance of

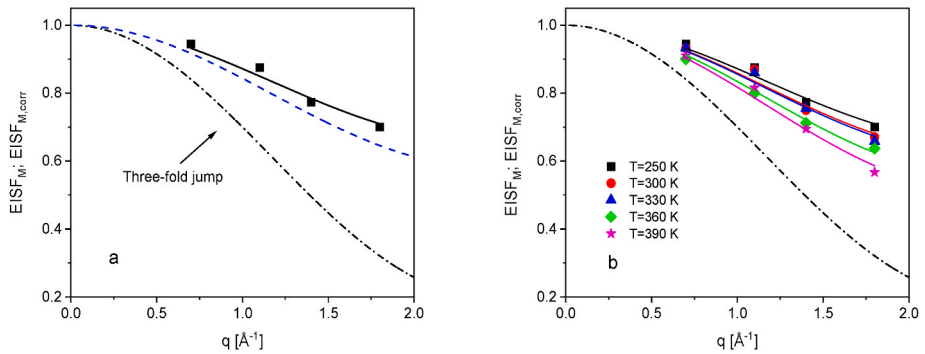

Fig. 8. $EISF_M$ and $EISF_{M,\,corr}$ versus the scattering vector q for ZMA66: a) At T = 250 K – dashed dotted EISF according to equ. 6. Blue dashed line – according to equ. 7 with the theoretical value of $C_{fix} = 0.478$. Black solid line – fit of equ. 7 to the data. b) At the indicated temperatures. Colored lines are fits of equ. 7 to the corresponding data. Dashed dotted EISF according to equ. 6. (For interpretation of the references to colour in this figure legend, the reader is referred to the Web version of this article.)

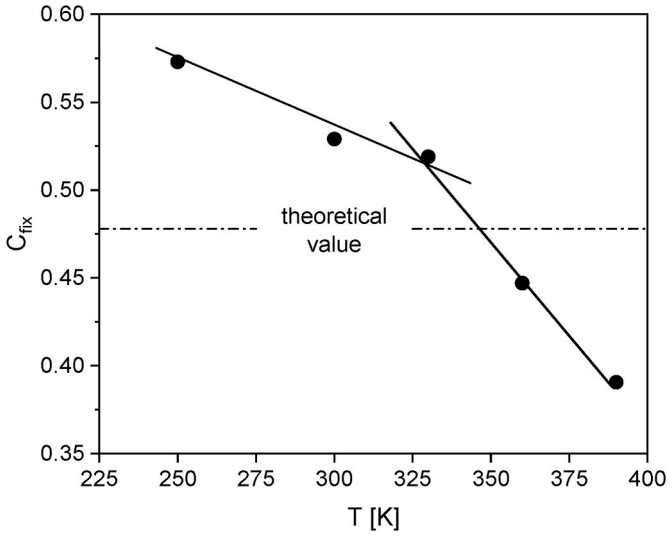

Fig. 9. C_{fix} versus temperature for ZMA66. The solid lines are guides for the eyes. The dashed-dotted line marks the theoretical values due to the chemical structure of the repeating unit. For the calculation of the theoretical value of C_{fix} see above.

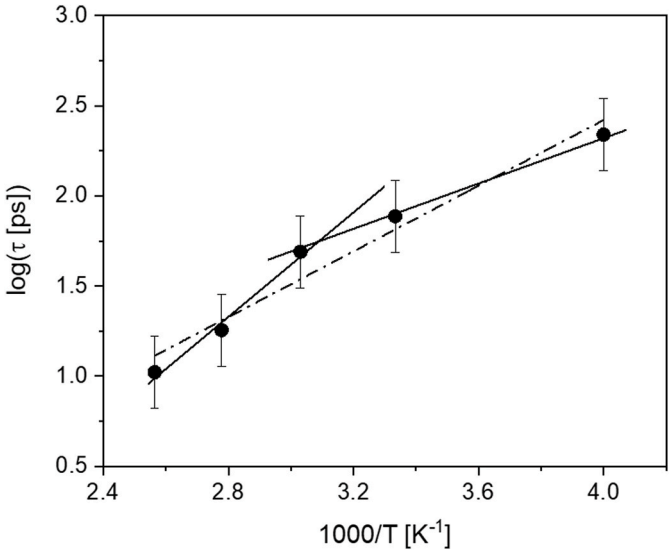

Fig. 10. Relaxation rate of the methyl group rotation versus inverse temperature for ZMA66. The dashed line is a linear regression to all data points. The regression coefficient of the linear regression including all points is $R^2 = 1$. The solid line indicates the change in the temperature dependence of the relaxation rates of the methyl group rotation.

polynorbornenes with bulky carbocyclic side groups. The low frequency vibrational density of states and the molecular mobility were estimated by a combination of inelastic and quasielastic neutron scattering.

For the inelastic neutron scattering the time-of-flight spectrometer FOCUS operated at the Swiss spallation source SINQ at the Paul Scherrer Institute was employed. It was shown that all polynorbornenes with bulky carbocyclic side groups considered in this study show a Boson peak. The correlation between the maximum frequency of the Boson peak and the microporosity, characterized by the value of the BET surface area, highlights the importance of structural features in determining the vibrational properties of these polymers.

Furthermore, the molecular mobility of two polynorbornenes obtained by metathesis polymerization was investigated by quasielastic neutron scattering. One main structural difference of both polymers considered is that one polymer has methyl groups in the side group whereas the other has none. To cover a reasonable dynamic range in the QENS experiments, neutron time-of-flight experiments were combined with neutron backscattering. For the time-of-flight measurements again the FOCUS was employed. For the neutron backscattering part of the experiment the spectrometer Emu (ANSTO, Lucas Heights, Australia) was utilized. The data obtained from both instruments were Fourier transformed and divided by the corresponding Fourier transform of their resolutions. By that approach both set of data could be jointly analyzed in the time domain. For the polymer having no methyl groups in the carbocyclic side group, only elastic scattering is observed in the considered temperature range. In contrast, for the polymer bearing methyl groups, one relaxation process was present in the intermediate incoherent scattering function. It was assigned to the methyl group rotation and analyzed in the framework of a jump diffusion in a three-fold potential. This analysis provides the correct q dependence of the elastic incoherent structure factor for the methyl group rotation when the amount of hydrogen taking part in the methyl group rotation is considered. It was also observed that the amount of methyl groups which participate in the rotation increases with temperature. The study provides deeper insights into the dynamics of the polymers, which is crucial for the fundamental understanding of transport processes related to molecular mobility of the polymer matrix, necessary for optimizing gas separation efficiency of such materials.

CRediT authorship contribution statement

Paulina Szymoniak: Writing – review & editing, Investigation, Data curation. **Mohamed A. Kolmangadi:** Data curation. **Martin Böhning:** Data curation. **Nicolas R. De Souza:** Data curation. **Fanni Juranyi:** Data curation. **Reiner Zorn:** Methodology, Data curation. **Andreas Schönhals:** Writing – original draft, Supervision, Investigation, Data curation, Conceptualization.

Declaration of competing interest

There is no conflict of interests.

Acknowledgments

We are grateful to Dr. Dmitry A. Alentiev, M. A, Zotkin, and Dr. Maxim Bermeshev (Moscow) providing the ZMA materials to us. This work is based on neutron time-of-flight experiments performed at the Swiss spallation neutron source SINQ, Paul Scherrer Institute, Villigen, Switzerland. The Australian Nuclear Science and Technology Organisation (ANSTO, Lucas Heights, Australia) is thanked for enabling the neutron back scattering experiments (ANSTO proposal number 13502).

Appendix A. Supplementary data

Supplementary data to this article can be found online at https://doi.org/10.1016/j.polymer.2025.128358.

Data availability

Data will be made available on reasonable request.

References

[1] R.W. Baker, Membrane Technology and Applications, John Wiley & Sons, Chichester, UK, 2004.
[2] Y. Yampolskii, Polymeric gas separation membranes *macromolecules* 45 (2012) 3298–3311.
[3] J.G. Wijmans, R.W. Baker, The solution-diffusion model: a review, J. Membr. Sci. 107 (1995) 1–21.
[4] B.J. Sundell, J.A. Lawrence, J.A. Iii, D.J. Harrigan, J.T. Vaughn, T.S. Pilyugina, D. R. Smith, Alkoxysilyl functionalized polynorbornenes with enhanced selectivity for heavy hydrocarbon separations, RSC Adv. 6 (2016) 51619–51628.
[5] J.T. Vaughn, D.J. Harrigan, B.J. Sundell, J.A. Lawrence Iii, J. Yang, Reverse selective glassy polymers for C3+ hydrocarbon recovery from natural gas, J. Membr. Sci. 522 (2017) 68–76.
[6] K.R. Gmernicki, E. Hong, C.R. Maroon, S.M. Mahurin, A.P. Sokolov, T. Saito, B. K. Long, Accessing siloxane functionalized polynorbornenes via vinyl-addition polymerization for CO_2 separation membranes, ACS Macro Lett. 5 (2016) 879–883.
[7] D.A. Alentiev, E.S. Egorova, M.V. Bermeshev, L.E. Starannikova, M.A. Topchiy, A. F. Asachenko, P.S. Gribanov, M.S. Nechaev, Y.P. Yampolskii, E.S. Finkelshtein, Janus tricyclononene polymers bearing Tri(n-Alkoxy)Silyl side groups for membrane gas separation, J. Mater. Chem. A (2018) 19393–19408.
[8] M. Kolmangadi, P. Szymoniak, G.J. Smales, D. Alentiev, M. Bermeshev, M. Böhning, A. Schönhals, Molecular dynamics of Janus polynorbornenes: glass transitions and nanophase separation, Macromolecules 53 (2020) 7410–7419.
[9] P. Szymoniak, M.A. Kolmangadi, F. Juranyi, M. Böhning, R. Zorn, Low -frequency vibrational density of state of Janus-polynorbornenes: the dependence of the Boson peak on the nanophase-separated structure, Macromolecules 56 (2023) 5803–5812.
[10] P. Szymoniak, M.A. Kolmangadi, M. Böhning, B. Frick, M. Appel, R.A. Mole, N. R. De Souza, R. Zorn, A. Schönhals, Confined segmental diffusion in nanophase separated Janus polynorbornenes as investigated by quasielastic neutron scattering, Macromolecules 57 (2024) 8562–8575.
[11] T. Higashimura, T. Masuda, M. Okada, Gas permeability of polyacetylenes with bulky substituents, Polym. Bull. 10 (1983) 114–117.
[12] T. Masuda, M. Kawasaki, Y. Okano, T. Higashimura, Polymerization of methylpentynes by transition metal catalysts: monomer structure, reactivity, and polymer properties, Polym. J. 14 (1982) 371–377.
[13] A. Morisato, I. Pinnau, Synthesis and gas permeation properties of Poly(4-methyl-2-pentyne), J. Membr. Sci. 121 (1996) 243–250.
[14] P.M. Budd, K.J. Msayib, C.E. Tattershall, B.S. Ghanem, K.J. Reynolds, N. B. McKeown, D. Fritsch, Gas separation membranes from polymers of intrinsic microporosity, J. Membr. Sci. 251 (2005) 263–269.
[15] M. Carta, R. Malpass-Evans, M. Croad, Y. Rogan, J.C. Jansen, P. Bernardo, F. Bazzarelli, N.B. McKeown, An efficient polymer molecular sieve for membrane gas separations, Science 339 (2013) 303–307.
[16] Y. Wang, B.S. Ghanem, Y. Han, I. Pinnau, State-of-the-art polymers of intrinsic microporosity for high-performance gas separation membranes, Curr. Opin. Chem. Eng. 35 (2022) 100755.
[17] R. Swaidan, B. Ghanem, E. Litwiller, I. Pinnau, Physical aging, plasticization and their effects on gas permeation in "rigid" polymers of intrinsic microporosity, Macromolecules 48 (2015) 6553–6561.
[18] D. Hofmann, M. Heuchel, Y. Yampolskii, V. Khotimskii, V. Shantarovich, Free volume distributions in ultrahigh and lower free volume polymers: Comparison between molecular modeling and positron lifetime studies, Macromolecules 35 (2002) 2129–2140.
[19] M. Heuchel, D. Fritsch, P.M. Budd, N.B. McKeown, D. Hofmann, Atomistic packing model and free volume distribution of a polymer with intrinsic microporosity (PIM-1), J. Membr. Sci. 318 (2008) 84–99.
[20] P.P. Chapala, M.V. Bermeshev, L.E. Starannikova, N.A. Belov, V.E. Ryzhikh, V. P. Shantarovich, V.G. Lakhin, N.N. Gavrilova, Y.P. Yampolskii, E.S. Finkelshtein, A novel, highly gas-permeable polymer representing a new class of silicon-containing polynorbornens as efficient membrane materials, Macromolecules 48 (2015) 8055–8061.
[21] M. Gringolts, M. Bermeshev, Y. Yampolskii, L. Starannikova, V. Shantarovich, E. Finkelshtein, New high permeable addition poly(tricyclononenes) with $Si(CH_3)_3$ side groups. Synthesis, gas permeation parameters, and free volume, Macromolecules 43 (2010) 7165–7172.
[22] M.A. Zotkin, D.A. Alentiev, S. Shorunov, S.E. Sokolov, N.N. Gavrilova, M. V. Bermeshev, Microporous polynorbornenes bearing carbocyclic substituents. Structure-property study, Polymer 269 (2023) 125732.
[23] D.A. Alentiev, M. Bermeshev, Design and synthesis of porous organic polymeric materials from norbornene derivatives, Polym. Rev. 38 (2021) 430–437, 6.
[24] M.A. Guseva, A.D. Alentiev, D.S. Bakhtin, I.L. Borisov, A.V. Volkov, E. S. Finkelshtein, M.V. Bermeshev, Polymers based on exo-silicon-substituted norbornenes for membrane gas separation, J. Membr. Sci. 638 (2021) 11956.
[25] X. Wang, T.J. Wilson, D. Alentiev, M. Gringolts, E.S. Finkelshtein, M. Bermeshev, B. K. Long, Substituted polynorbornene membranes: a modular template for targeted gas separations, Polym. Chem. 12 (2021) 2947–2977.
[26] A. Fuoco, C. Rizzuto, E. Tocci, M. Monteleone, E. Esposito, P.M. Budd, M. Carta, B. Comesañ-Gándara, N.B. McKeown, J.C. Jansen, The origin of size-selective gas transport through polymers of intrinsic microporosity, J. Mater. Chem. A 7 (2019) 20121–20126.
[27] T. Kanaya, M. Teraguchi, T. Masuda, K. Kaji, Local Mobility of Substituted Polyacetylenes Measured by Quasielastic Neutron Scattering and Its Relationship with Gas Permeability *Polymer*, vol. 40, 1999, pp. 7157–7161.
[28] H. Yin, Y. Chua, B. Yang, C. Schick, W. Harrison, P.M. Budd, M. Böhning, A. Schönhals, First clear-cut experimental evidence of a glass transition in a polymer with intrinsic microporosity: PIM-1, J. Chem. Phys. Lett 9 (2018) 2003–2008.
[29] H. Yin, B. Yang, Y.Z. Chua, P. Szymoniak, M. Carta, R. Mallpass-Evans, N. McKeown, W.J. Harrison, P.M. Budd, C. Schick, M. Böhning, A. Schönhals, Effect of backbone rigidity on the glass transition of polymers of intrinsic microporosity probed by fast scanning calorimetry, ACS Macro Lett. 8 (2019) 1022–1028.
[30] M.A. Kolmangadi, P. Szymoniak, R. Zorn, M. Böhning, M. Wolf, M. Zamponi, A. Schönhals, Molecular mobility in high performance polynorbornenes: a combined broadband dielectric, advanced calorimetry, and neutron scattering investigations, Polym. Eng. Sci. 62 (2022) 2143–2155.
[31] N. Konnertz, Y. Ding, J.W. Harrison, P.M. Budd, M. Böhning, Molecular mobility of the high performance membrane polymer PIM-1 as investigated by dielectric spectroscopy, ACS Macro Lett. 5 (2016) 528–532.
[32] F. Emamverdi, H. Yin, G.J. Smales, W.J. Harrison, P.M. Budd, M. Böhning, A. Schönhals, Polymers of intrinsic microporosity – molecular mobility and physical aging revisited by dielectric spectroscopy and X-Ray scattering, Macromolecules 55 (2022) 7340–7350.
[33] H. Yin, P. Chapala, M. Bermeshev, B.R. Pauw, A. Schönhals, M. Böhning, Influence of trimethylsilyl side groups on the molecular mobility and charge transport in highly permeable glassy polynorbornenes, ACS Appl. Polym. Mater. 1 (2019) 844–855.
[34] H. Yin, P. Chapala, M. Bermeshev, A. Schönhals, M. Böhning, ACS Macro Lett. 6 (2017) 813–818.
[35] R. Inoue, T. Kanaya, T. Masuda, K. Nishida, O. Yamamuro, Relationship between the local dynamics and gas permeability of para-substituted Poly(1-chloro-2-phenylacetylenes), Macromolecules 45 (2012) 6008–6014.
[36] T. Kanaya, T. Kawaguchi, K. Kaji, T. Sakaguchi, G. Kwak, T. Masuda, Role of local dynamics in the gas permeability of glassy substituted polyacetylenes. A quasielastic neutron scattering, Study Macromolecules 35 (2002) 5559–5564.
[37] R. Zorn, W. Lohstroh, M. Zamponi, W.J. Harrison, P. Budd, M. Böhning, A. Schönhals, Molecular mobility of a polymer of intrinsic microporosity revealed by quasielastic neutron scattering, Macromolecules 53 (2020) 6731–6739.
[38] A. Schönhals, P. Szymoniak, M.A. Kolmangadi, M. Böhning, M. Zamponi, B. Frick, M. Appel, G. Günther, M. Russina, D.A. Alenttiev, M. Bermeshev, R. Zorn, Microscopic dynamics of highly permeable super glassy polynorbornenes revealed by neutron scattering, J. Membr. Sci. 642 (2022) 119972.
[39] R. Zorn, H. Yin, W. Lohstroh, W. Harrison, P.M. Budd, B.R. Pauw, M. Böhning, A. Schönhals, Anomalies in the low frequency vibrational density of states for a polymer with intrinsic microporosity – the boson peak of PIM-1, Phys. Chem. Chem. Phys. 20 (2018) 1355–1363.

[40] R. Zorn, P. Szymoniak, M.A. Kolmangadi, R. Malpass-Evans, N.B. McKeown, M. Tyagi, M. Böhning, A. Schönhals, Low frequency vibrations and diffusion in disordered polymers bearing an intrinsic microporosity as revealed by neutron scattering, Crystals 11 (2021) 1482.
[41] R. Zorn, P. Szymoniak, M. Kolmangadi, M. Wolf, D. Alentiev, M. Bermeshev, M. Böhning, A. Schönhals, Low frequency vibrational density of state of highly permeable super glassy polynorbornenes – the boson peak, Phys. Chem. Chem. Phys. 22 (2020) 8381–18387.
[42] M.A. Zotkin, D.M. Alenttiev, S.V. Shornov, S.E. Sokolov, N.N. Gavrilova, M. V. Bermeshv, Microporous polynorbornenes bearing carbocyclic substituents: structure-Property study, Polymer 269 (2023) 125732.
[43] M.A. Zotkin, D. Alenttiev, R.S. Borisov, A.A. Kozlova, I.L. Borisov, M.G. Shalygin, M.V. Bermeshev, Polynorbornenes with carbocyclic substituents: a perspective approach to highly permeable gas separation membranes, J. Membr. Sci. 702 (2024) 122786.
[44] M. Bée, Quasielastic Neutron Scattering: Principles and Applications in Solid State Chemistry, Biology and Materials Science, Adam Hilger Publishing House, 1988.
[45] R.T. Azuah, L.R. Kneller, Y. Qiu, P.L.W. Tregenna-Piggott, C.M. Brown, J.R. D. Copley, V.J. Dimeo, DAVE: a comprehensive software suite for the reduction, visualization, and analysis of low energy neutron spectroscopic data. Res, Natl. Inst. Stan. Technol. 114 (2009) 341.
[46] R. Zorn, Multiple scattering correction of neutron scattering elastic scans, Nucl. Instrum. Methods A 572 (2007) 874–881.
[47] R. Zorn, B. Frick, L. Fetters, Quasielastic neutron scattering study of the methyl group dynamics in polyisoprene, J. Chem. Phys. 116 (2002) 845–853.
[48] O. Arnold, et al., Mantid — data analysis and visualization package for neutron scattering and μSR experiments, Nucl. Instrum. Methods Phys. Res., Sect. A 764 (2014) 156–166.
[49] R. Zallen, The Physics of Amorphous Solids, Wiley, New York, 1983.
[50] C. Krause, R. Zorn, F. Emmerling, J. Falkenhagen, B. Frick, P. Huber, A. Schönhals, Vibrational density of states of triphenylene based discotic liquid crystals: dependence on the length of the alkyl chain, Phys. Chem. Chem. Phys. 16 (2014) 7324–7333.
[51] A.I. Krichikov, A. Jezowski, D. Szewczyk, O.A. Korolyuk, O.O. Romantsova, L. M. Buravtseva, C. Cazoria, J. Ll Tamarit, Role of optical phonons and anharmonicity in the appearance of the heat capacity boson peak-like anomaly in fully ordered molecular crystals, J. Phys. Chem. Lett. 13 (2022) 5061–5067.
[52] Y. Miyazaki, M. Nakano, A.I. Krivchikov, O.A. Koroyuk, J.F. Gebbia, C. Cazorla, J. Ll Tamarit, Low-temperature heat capacity anomalies in ordered and disordered phases of normal and deuterated thiophene, J. Phys. Chem. Lett. 12 (2021) 2112–2117.
[53] P. Lunkenheimer, A. Loidl, High-frequency excitations in glassy crystals, J. Non-Crys. Solids 352 (2006) 4556–4561.
[54] V.K. Malinovsky, V.N.A.P. Novikov, A.P. Sokolov, Investigation of structural correlations in disordered materials by raman scattering measurements, J. Non-Cryst. Solids 90 (1987) 485–488.
[55] U. Buchenau, Y.M. Galperin, V.L. Gurevich, A.D. Parshin, M.A. Ramos, H. R. Schober, Interaction of soft modes and sound waves in glasses, Phys. Rev. B Condens. Matter 46 (1992) 2798–2808.
[56] B.B. Laird, H.R. Schober, Localized low-frequency vibrational modes in a simple model glass, Phys. Rev. Lett. 66 (1991) 636–639.
[57] S.N. Taraskin, Y.L. Loh, G. Natarajan, S.R. Elliott, Origin of the boson peak in systems with lattice disorder, Phys. Rev. Lett. 86 (2001) 1255–1258.
[58] V.K. Malinovsky, A.P. Sokolov, The nature of the boson in raman scattering in glasses, Solid State Commun. 57 (1986) 757–761.
[59] V.K. Malinovsky, V.N. Novikov, A.P. Sokolov, V.A. Bagryansky, Light scattering by fractons, Chem. Phys. Lett. 143 (1988) 111–114.
[60] L. Hong, V.N. Novikov, A.P. Sokolov, Dynamic heterogeneities, boson peak, and activation volume in glass-forming liquids, Phys. Rev. E 83 (2011) 061508.
[61] W. Schirmacher, G. Diezemann, C. Ganter, Harmonic vibrational excitations in disordered solids and the "boson peak", Phys. Rev. Lett. 81 (1998) 136–139.
[62] Y. Wang, L. Hong, Y. Wang, W. Schirmacher, J. Zhang, Disentangling boson peaks and Van hove singularities in a model glass", Phys. Rev. B 98 (2018) 174207.
[63] M. Gonzalez-Jimenez, T. Barnard, B.A. Russell, N.V. Tukachev, U. Javonik, L.-A. Hayes, A.J. Farrell, S. Guinane, H.M. Senn, A.J. Smith, M. Wilding, G. Mali, M. Nakano, Miyazaki, P. McMillan, G.C. Sosso, K. Wynne, Understanding the emergence of the boson peak in molecular glasses, Nat. Commun. 14 (2023) 215.
[64] E. Lerner, E. Bouchbinder, Boson-peak vibrational modes in glasses feature hybridized phononic and quasilocalized excitations, Cond-Mat.Soft (2023) 10326 arXiv:2210.
[65] R. Milkus, A. Zaccone, Local inversion-symmetry breaking controls the boson peak in glasses and crystals, Phys. Rev. B 93 (2016) 094204.
[66] A. Schönhals, R. Zorn, B. Frick, Inelastic neutron spectroscopy as a tool to investigate nanoconfined polymer systems *polymer* 105 (2016) 393–406.
[67] R. Zorn, M. Mayorova, D. Richter, A. Schönhals, L. Hartmann, F. Kremer, B. Frick, Effect of nanoscopic confinement on the microscopic dynamics of glass-forming liquids and polymers studied by inelastic neutron scattering, AIP Conf. Proc. 982 (2008) 79–84.
[68] T. Asthalter, M. Bauer, U. van Bürck, I. Sergueev, H. Franz, A.I. Chumakov, Confined phones in glasses, Eur. Phys. J. E: Soft Matter Biol. Phys. 12 (2003) S9–S12.
[69] A. Schönhals, H. Goering, C. Schick, B. Frick, R. Zorn, Glass transition of polymers confined to nanoporous glasses, Colloid Polym. Sci. 282 (2004) 882–891.
[70] R. Zorn, Phys. Rev. B: Condens. Matter Mater. Phys., Boson peak in confined disordered systems 81 (2010) 054208.
[71] P. Szymoniak, M.A. Kolmangadi, F. Juranyi, M. Böhning, R. Zorn, A. Schönhals, Low-frequency vibrational density of state of janus-polynorbornenes: the dependence of boson peak on the nanophase-separated structure, Macromolecules 56 (2023) 5803–5812.
[72] S.W. Lovesey, Theory of Neutron Scattering from Condensed Matter, vol. 1, Oxford University, New York, 1987, p. 121.
[73] R. Zorn, L. Hartmann, B. Frick, D. Richter, F. Kremer, J. Non-Cryst. Solids 307 (2002) 547–554.
[74] J. Colmenero, A. Moreno, A. Alegria, Prog. Polym. Sci. 30 (2005) 1147–1184.
[75] M. Prager, A. Heidemann, Rotational tunneling and neutron spectroscopy: a compilation, Chem. Rev. 97 (1997) 2933–2966.
[76] A. Schönhals, Ch Schick, H. Huth, B. Frick, M. Mayorova, R. Zorn, Molecular dynamics in glass-forming poly(phenyl methyl siloxane) as investigated by broadband thermal, dielectric and neutron spectroscopy, J. Non-Cryst. Solids 353 (2007) 3853–3861.